Journal of Molecular Liquids 428 (2025) 127498

Contents lists available at ScienceDirect

Journal of Molecular Liquids

journal homepage: www.elsevier.com/locate/molliq

Green synthesis of copper ferrite-based nanofluids using *Chlorella vulgaris* for heat transfer enhancement

Beatriz Cardoso [a], Glauco Nobrega [a,b,*], Mariana Machado [a], Rui A. Lima [a,c,d]

[a] Mechanical Engineering and Resource Sustainability Center (MEtRICs), Mechanical Engineering Department, University of Minho, Campus de Azurém, 4800-058 Guimarães, Portugal
[b] Centro de Investigação de Montanha (CIMO), Instituto Politécnico de Bragança, Campus de Santa Apolónia, 5300-253 Bragança, Portugal
[c] Transport Phenomena Research Center (CEFT), Faculdade de Engenharia da Universidade do Porto (FEUP), Rua Roberto Frias, 4200-465 Porto, Portugal
[d] Faculty of Engineering, Associate Laboratory in Chemical Engineering (ALiCE), University of Porto 4200-465 Porto, Portugal

ARTICLE INFO

Keywords:
Green-synthesis
Metallic nanoparticles
Chlorella vulgaris
Biosynthesis
Heat transfer
Thermal conductivity

ABSTRACT

This study investigates the green synthesis of copper ferrite nanoparticles ($CuFe_2O_4$ NPs) using an aqueous extract of *Chlorella vulgaris* as a reducing agent and their application in enhancing heat transfer through nanofluids. The successful formation of $CuFe_2O_4$ NPs was confirmed through UV–vis spectroscopy, revealing a progressive blue shift in absorption peaks from 380 nm to 350 nm over 4 h, accompanied by a reduction in band gap energy from 2 eV to 1.83 eV, indicating increased particle size and crystallinity. Scanning electron microscopy demonstrated relatively uniform morphology with an average particle size of 130 nm. The EDS analysis revealed strong Cu, Fe, and O peaks, consistent with the expected spinel ferrite composition. Water-based nanofluids containing 0.1 wt%, 0.5 wt%, and 1 wt% $CuFe_2O_4$ NPs were prepared and characterized. The 1 wt% nanofluid showed a 4.8 % improvement in thermal conductivity compared to water, while viscosity remained within a manageable range (~1.1 mPa·s), ensuring low pumping power requirements. In heat transfer experiments using a serpentine heat exchanger, the $CuFe_2O_4$ 1 wt% nanofluids achieved a significant increase in heat absorption capacity, increasing the outlet temperature by at least 0.5 °C at all volumetric flow rates tested and with a significant improvement in heat storage capacity at the highest flow rate. These results highlight the efficacy of green-synthesized $CuFe_2O_4$-based nanofluids in significantly improving heat transfer performance while maintaining practical fluid properties, making them ideal for sustainable and efficient thermal management applications, and suitable for monophasic and biphasic applications.

1. Introduction

Over the last decade, the scientific community has been investigating new and more effective cooling mechanisms, with the heat transfer process being one of the most important at an industrial level. Nanofluids are colloidal suspensions of nanoparticles (NPs) in base fluids (e.g., water, ethylene glycol) and have demonstrated enhanced thermal conductivity and convective heat transfer performance compared to conventional fluids [1,2]. This improvement is attributed to mechanisms such as increased mass flow rate, enhanced thermal conductivity due to NPs Brownian motion, which induces micro-convection and increases thermal conductivity. As temperature rises, the increased movement and collisions of NPs further enhance this effect. The reduction of boundary layer thickness and particle clustering, the high surface-to-volume ratio and inherent thermal conductivity of the NPs themselves contribute to the observed improvement in thermal conductivity with increasing NPs volume fraction, among others [3–5].

Nanofluids have been applied in several fields, including industries of power generation, where they facilitate efficient heat transfer in plants and equipment [6]; automotive industries, enhancing vehicle cooling systems [7]; and aerospace, improving thermal management of electronic components in spacecraft and aircraft [8,9]. Several NPs, including iron oxide [10–12], titania [13,14], zinc oxide [15,16], and copper oxide [17,18], have been studied for their suitability in formulating nanofluids.

Among these, copper ferrite NPs ($CuFe_2O_4$ NPs) have attracted

* Corresponding author at: Mechanical Engineering and Resource Sustainability Center (MEtRICs), Mechanical Engineering Department, University of Minho, Campus de Azurém, 4800-058 Guimarães, Portugal.
E-mail addresses: glaucotvn@hotmail.com, nobregaglauco@gmail.com (G. Nobrega).

https://doi.org/10.1016/j.molliq.2025.127498
Received 1 October 2024; Received in revised form 28 March 2025; Accepted 31 March 2025
Available online 2 April 2025

significant attention due to their high thermal conductivity, magnetic properties, and thermal stability [2,19]. Their unique physicochemical characteristics result from their inverse cubic crystalline structure, where Cu ions occupy tetrahedral zones and Fe ions occupy octahedral zones, contributing to their superior performance in heat transfer systems [20–22]. Experimental studies have confirmed that $CuFe_2O_4$-based nanofluids significantly enhance convective heat transfer coefficients, as indicated by improved Nusselt numbers [19].

NP synthesis methods include physical, chemical, and green synthesis approaches. While physical and chemical methods dominate, they present challenges such as toxic solvent use, environmental impact, and high energy demands [23,24]. In contrast, green synthesis, which employs biological resources like plant extracts, microorganisms, and waste materials, offers a sustainable alternative [24–26]. It produces well-defined NPs with controlled size and morphology, using eco-friendly processes with low energy requirements and minimal environmental impact [23]. Furthermore, NPs synthesized via green methods have demonstrated significant potential for application in thermal nanofluids due to their enhanced stability within the colloidal mixture compared to chemically synthesized particles, along with superior thermal capacity and stability [27].

Microalgae and macroalgae have emerged as promising resources for green synthesis due to their richness in bioactive compounds, such as chlorophyll and antioxidants, which act as reducing and stabilizing agents during NP formation [28]. These phytochemicals act as reducing and surface functionalization (capping) agents in synthesizing metallic NPs and play a crucial role in their stabilization. *Chlorella vulgaris*, a microalgae, has been used to synthesize metallic NPs such as gold, silver, and palladium, but its application in $CuFe_2O_4$ synthesis remains underexplored [28].

This study aimed to advance knowledge in green synthesis by using *Chlorella vulgaris* extract to produce $CuFe_2O_4$ NPs and assess their application in heat transfer nanofluids. The synthesized NPs were incorporated into water-based nanofluids at concentrations of 0.1 wt%, 0.5 wt%, and 1 wt%, which were then characterized for wettability, viscosity, thermal conductivity, and heat transfer performance. The influence of $CuFe_2O_4$ NPs on nanofluid properties and their potential for single-phase and two-phase heat exchange systems were comprehensively evaluated, highlighting the feasibility of eco-friendly nanofluids in industrial heat transfer applications.

2. Materials and methods

2.1. Apparatus and materials

This work used *Chlorella vulgaris* as biomass for the green synthesis of $CuFe_2O_4$ NPs. *Chlorella vulgaris* was obtained from ALLMA®. The pH value was measured with the APERA Instruments PH20 meter, and the pH of each solution was correctly adjusted with a 1 M sodium hydroxide (NaOH) solution (Sigma-Aldrich, St. Louis, MO, USA). Iron (II) chloride tetrahydrate 98 % *Thermoscientific*™ and copper (II) sulfate hydrate 98 % *Sigma-Aldrich*® were used as reagents.

A mold was conceived and subsequently printed in an *Anycubic Photon D2 DLP resin 3D printer to fabricate the serpentine*. The transparent PDMS Sylgard 184 was used as the winding material. This material was selected due to its incredible capacity to reproduce mold surfaces, non-toxicity, chemical resistance, and simple preparation that does not require previous knowledge or a particular machine with high pressure and/or temperature, as silicone used needs to be transparent, as previously mentioned. The PDMS was prepared with a 10:1 proportion with the curing agent using the same protocol applied by [29]. To perform the heat transfer experiment, a Peristaltic Pump *New Era NE-9000* was applied to generate the controlled fluid flow, reservoir *Vesta Perfecta Water Bath* was utilized to keep the fluids at the desired temperature, *DC Lab Switching Power Supply LABPS6005SM velleman*® supplied the current to a 0.2 mm sheet of stainless steel (AISI 3049). The temperature was registered by *TC-08 Thermocouple Data Logger, Pico®Technology*, through thermocouple type "T" inserted in the fluid inlet, outlet, and at the stainless-steel sheet. Acrylic plates and screws with nuts were used to assemble the system. Although most heat exchangers are made of conductive metals such as aluminum or cuppers, this test was carried out with a PDMS coil to observe the behavior of the nanofluid while it was being tested [30].

2.2. Biosynthesis of copper ferrite nanoparticles using Chlorella vulgaris

2.2.1. Preparation of Chlorella vulgaris extract

To prepare the aqueous extract of *Chlorella vulgaris*, 3.5 g of *Chlorella vulgaris* algae powder was added to 50 mL of distilled water. The aqueous solution was heated to 55 °C under magnetic stirring for 30 min and then placed in an ultrasound for 10 min. The cycle was repeated three times (according to Fig. 1). Then, the solution was centrifuged twice at 4000 rpm for 20 min to separate biological residues from the extract. Whatman No. 1 filter paper filtered the supernatant resulting from centrifugation, resulting in the aqueous extract being stored at 4 °C for future use.

2.2.2. Preparation of copper ferrite nanoparticles

For the preparation of $CuFe_2O_4$ NPs, 0.2 M of iron (III) chloride solution and 0.1 M of copper (II) sulfate (2:1 M ratio) were added to 90 mL of distilled water. Then, 10 mL of the previously obtained aqueous extract of *Chlorella vulgaris* was added to the metal precursors solution, drop by drop, using a syringe pump (*New Era NE-300*), under continuous magnetic stirring. The dropwise addition ensures a slow reaction between the *Chlorella vulgaris* aqueous extract and the metal precursors solution. The mixture was incubated at 60 °C to carry out for 60 min. Then, the reaction was adjusted to pH = 11 using a NaOH solution at 1 M. Several aliquots at 1 h, 2 h, 3 h, and 4 h were collected over the reaction time. After some time, the solution changed color (green to brown), indicating the formation of $CuFe_2O_4$ NPs. Then, the synthesized NPs were purified through repeated washing and centrifugation cycles to remove residual reaction byproducts. After each centrifugation step (4000 rpm, room temperature, 10 min), the supernatant was carefully discarded, and the NPs were resuspended in distilled water. This process was repeated five times to ensure thorough cleaning of the NPs. Following the final wash, the NPs were suspended in 100 mL of distilled water. Due to their tendency to become unstable when fully dried—primarily because of agglomeration or structural changes resulting from the loss of the stabilizing aqueous medium—the NPs were maintained in aqueous suspension after purification and were not subjected to complete drying. To quantify the concentration of NPs in the suspension, a 5 mL aliquot was withdrawn and dried to constant weight. The mass of the dried NPs was then used to calculate the total NPs concentration in the suspension. This method ensured precise quantification while preserving the stability of the NPs in their aqueous form.

2.3. Characterization of copper ferrite nanoparticles and copper ferrite nanoparticles nanofluids

To follow the synthesis of $CuFe_2O_4$ NPs over time, the peak absorption of the aliquots was monitored using a UV-1800 UV–Vis spectrometer. Furthermore, all samples' band gap energy (eV) over time was determined using Eq. (1).

$$(\alpha h\upsilon)^{\frac{1}{n}} = A(h\upsilon - E_g) \tag{1}$$

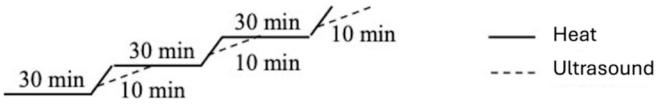

Fig. 1. Heating/ultrasound cycle during Chlorella vulgaris extract preparation.

where α is the absorption coefficient, υ is light frequency, h is Planks constant, and E_g is band gap. The band gap value is calculated by the curve of the line to the x-axis.

The Scanning electron microscopy (SEM) images of $CuFe_2O_4$ NPs were obtained using a FlexSEM 1000 scanning electron microscope, operating at an accelerating voltage of 10 kV. Initially the NPs were dispersed in an alcohol solution then a small amount of the solution was then deposited in a conductive carbon adhesive tape and put in onto aluminum stubs. To ensure electrical conductivity and prevent charge buildup during SEM analysis, the samples were coated with a thin layer of gold with 7.5 nm using a Quorum Mini QS sputter coater.

EDS analysis of the $CuFe_2O_4$ NPs sample was carried out using Energy Dispersive X-ray Spectroscopy (EDS). EDS analysis was performed on randomly selected regions of the sample surface to ensure representative data. The measurements were conducted at an acceleration voltage ranging of 10 kV. This approach allowed for precise elemental composition analysis of the NPs.

After the synthesis and purification of the NPs, nanofluid samples were prepared containing 0.1 wt%, 0.5 wt%, and 1 wt% of $CuFe_2O_4$ NPs in water (base fluid). Then, the wettability of each nanofluid was assessed, which was measured using the DataPhysics OCA – Series at room temperature (23 °C). The wettability of each sample was evaluated on two substrates, PDMS produced according to [29] and aluminum (AL6070-T6, roughness 4.489 μm). For that, 10 μL of each nanofluid was dispensed onto the corresponding substrate, where 30 measurements were carried out in six different positions for each substrate. The average and standard deviation of each sample's wettability were calculated. Finally, the viscosity of each nanofluid was measured using an MCR 92 rotational rheometer (Anton Paar). A dish with conical geometry was used with a diameter of 50 mm and an opening of 1 mm. The shear flow curves were obtained at a constant temperature of 20 °C. To obtain reproducibility, three replicates of each measurement were evaluated.

2.4. Nanofluids thermal conductivity and heat exchanger capacity

Measurements of the thermal conductivity of each nanofluid were carried out using the transient plane source method with a Hot Disk TPS 2500S, using the Hot Disk 5501 F1 sensor and the fluid closed in a PDMS cell designed for thermal conductivity measurements of nanofluids, according to [29]. Five measurements were performed for each sample, and all measurements were conducted at 20 °C. The heat exchange capacity of the nanofluids, more precisely the thermal absorption capacity of the nanofluid, was carried out using a PDMS-based serpentine designed according to [30]. The tests were carried out at a temperature of 25 °C with three flow rates, 5, 10, and 15 mL/min. Fig. 2 shows a representative diagram of the assembly of the PDMS-based heat exchanger (serpentine).

To determine the heat flow rate (Q ̇) to the fluid, it is necessary to know the mass flow rate (m ̇), the heat capacity (Cp), and the temperature variation (ΔT) as shown in Eq. (2).

$$\dot{Q} = \dot{m} \times Cp \times \Delta T[W] \tag{2}$$

where $\dot{Q}$ is the Power transferred to the fluid, $\dot{m}$ is the mass flow [kg/s], Cp is the specific heat [J/kg. K] and ΔT is the temperature variation [K].

To determine the Cp of nanofluid the mixture rule [31] was applied as shown in Eq. (3).

$$(C_p)_{nf} = \frac{(1-\phi_{np})(\rho C_p)_{bf} + \phi_{np}(\rho C_p)_{nP}}{(1-\phi_{nP})\rho_{bf} + \phi_{nP}\rho_{nP}} \tag{3}$$

where ϕ_{np} is the volume percentage of nanoparticles, ρ is the density [kg/m^3], and Cp is the specific heat [J/kg. K]. The subscript nf is reference for "nanofluid", bf for "base fluid" and nP for "nanoparticle". In the present work, de density and specific heat of nanoparticles used were 5400 kg/m^3 and 720 J/kg·K [32], respectively.

3. Results and discussion

3.1. Biosynthesis and optical studies of copper ferrite nanoparticle

The synthesis of $CuFe_2O_4$ NPs was achieved through the reduction of metal precursors, specifically iron chloride and copper sulfate, by biomolecules present in the aqueous extract of *Chlorella vulgaris*. The initial indication of NP formation was the distinct color change in the reaction solution, transitioning from orange to brownish. This color progressively darkened over the reaction, reaching a deeper shade by the 4 h mark, a characteristic feature of $CuFe_2O_4$ NPs (Fig. 3) [33]. This color transition became progressively more pronounced as the reaction proceeded, ultimately deepening to a dark brown shade. Further evidence of successful synthesis was provided by the magnetic properties of the NPs, which allowed them to be easily separated using an external permanent magnet. This behavior confirmed the formation of magnetic $CuFe_2O_4$ NPs.

To monitor the progression of NP synthesis, UV–vis absorption n spectra of reaction aliquots were recorded over the 200–800 nm wavelength range (Fig. 4**A**). The results showed a continuous increase in the intensity of the absorption peaks with reaction time, indicating the ongoing reduction of iron chloride and copper sulfate into $CuFe_2O_4$ NPs. Moreover, a blue shift in the absorption peak was observed—from 380 nm at 1 h to 350 nm at 4 h. This shift toward higher energy wavelengths suggests changes in NPs size and shape, likely influenced by continued nucleation and growth processes [34]. This also suggests chemical changes occurring on the surface of the NPs over time, likely due to the binding of hydrophilic capping agents present in the algae extract [25,35]. The binding of these capping agents reduces NPs aggregation, a phenomenon that is also reflected in the observed blue shift [36]. Based on the absorption intensity data, the reaction was observed to progress steadily up to 4 h, indicating that the $CuFe_2O_4$ NPs were formed and

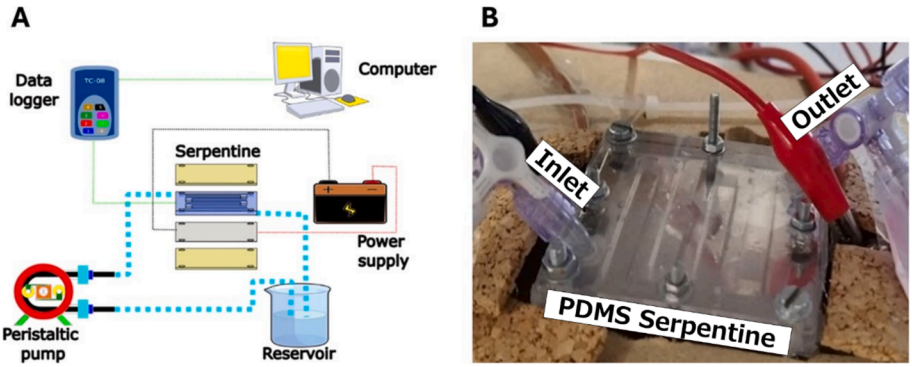

Fig. 2. (A) Schematic representation of the heat exchanger capacity assay assembly diagram and (B) real image of heat exchanger.

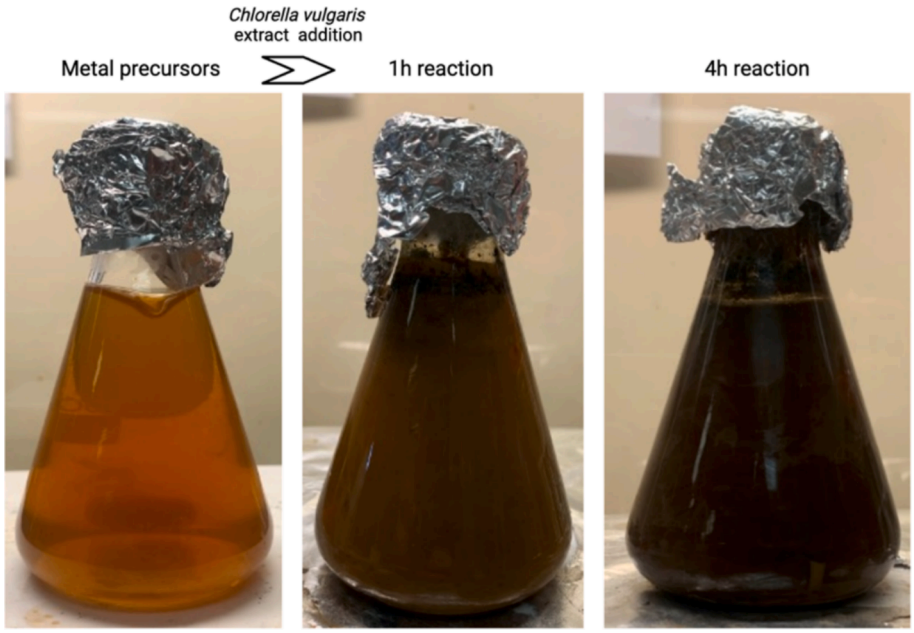

Fig. 3. Color evolution during the synthesis of $CuFe_2O_4$ NPs using *Chlorella vulgaris* extract: Initial orange solution of metal precursors (left) gradually darkens to a brownish color after 1 h of reaction (center) and further deepens into a darker shade after 4 h of reaction (right), indicating nanoparticle formation.

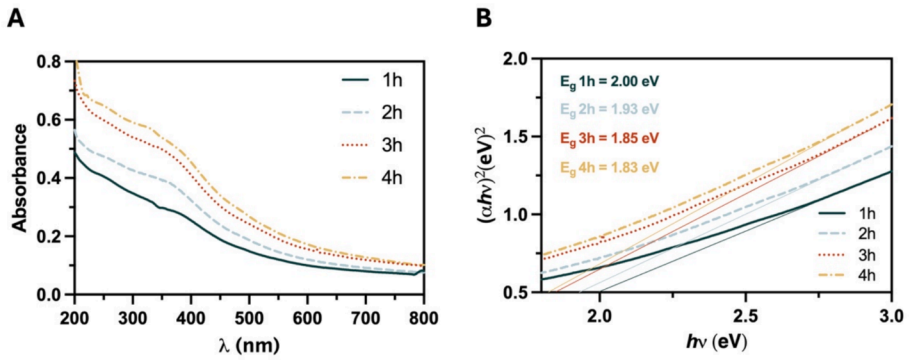

Fig. 4. (A) UV–Vis absorption spectra and (B) band gap energy of $CuFe_2O_4$ NPs during the synthesis reaction times of 1 h, 2 h, 3 h, and 4 h.

stabilized during this time. The slight difference observed between 3 h and 4 h could be attributed to the final stages of the reaction, where the formation rate slows down as the reaction approaches completion.

The band gaps of the $CuFe_2O_4$ NPs were calculated at various synthesis reaction times, as summarized in Fig. 4**B**, and showed a decreasing trend with increasing reaction time. At 1 h, the band gap was larger, suggesting smaller NPs due to the stronger quantum confinement effect, which is known to increase band gap energy [37,38]. As the reaction progressed, the growth of $CuFe_2O_4$ NPs reduced the quantum confinement effect, resulting in a gradual decrease in the band gap from 2 eV to 1.83 eV. In addition to particle size, surface defects, and non-stoichiometric compositions in the early stages of synthesis contribute to states within the band gap, leading to higher band gap values [39,40]. With longer synthesis times, these defects are minimized, improving the crystallinity and yielding a band gap closer to the intrinsic bulk value. This trend aligns with the observed blue shift in absorption spectra, as reduced surface defects and improved stoichiometric control may offset the effect of increasing particle size, resulting in a shift toward higher energy wavelengths.

3.2. Scanning electron microscopy and energy dispersive spectroscopy analysis of copper ferrite nanoparticles

The morphology and structural properties of $CuFe_2O_4$ NPs were characterized through SEM and size distribution analysis (Fig. 5). SEM images revealed dense agglomerates of NPs with relatively uniform morphology. The particle size distribution, derived from SEM images analysis using ImageJ software, exhibited a Gaussian profile with an average size of 130.1 ± 26.0 nm. These sizes are similar to those obtained by Sravanthi *et al.* [41], who synthesized CuO NPs using *Antigonon leptopus* leaf extract, reporting clustered particles with sizes ranging from 110 to 280 nm. However, other studies have demonstrated significantly smaller NPs sizes, underscoring the influence of synthesis conditions and the composition of plant extracts. For instance, Khatami *et al.* [42] synthesized CuO NPs with sizes between 17 and 41 nm using *Capparis spinosa* fruit extract, while Alhalili [43] reported particle sizes of approximately 88 nm using plant-derived capping agents.

The observed differences in NPs size and morphology across these studies can be attributed to variations in reaction parameters such as temperature, pH, precursor concentration, and the type and concentration of bioactive compounds in plant extracts [44]. Capping agents present in the extracts, such as flavonoids, phenols, and polysaccharides, play a crucial role in stabilizing nanoparticles, inhibiting overgrowth,

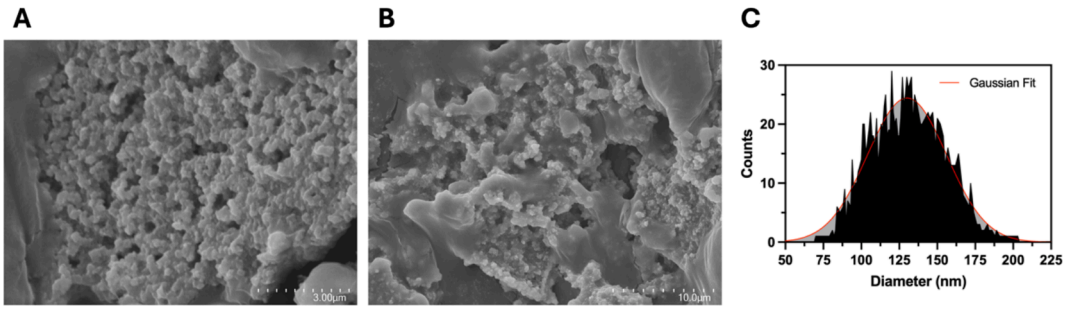

Fig. 5. (A) and (B) SEM images of $CuFe_2O_4$ NPs synthesized using *Chlorella vulgaris* extract taken at 3 μm and 10 μm, respectively; (C) Nanoparticle size distribution analysis, including particle count and Gaussian curve fitting, derived from SEM image analysis using ImageJ software.

and preventing aggregation in colloidal solutions [35]. In this study, the size of $CuFe_2O_4$ NPs may be attributed to the specific bioactive profile of the *Chlorella vulgaris* extract, which influences both the nucleation and growth processes during synthesis.

The elemental composition of the synthesized $CuFe_2O_4$ NPs was confirmed by EDS, as shown in Fig. 6. The spectrum exhibits distinct peaks for copper (Cu), iron (Fe), and oxygen (O), validating the successful formation of $CuFe_2O_4$. The Cu peaks at ~ 8.1 keV (Kα) and ~ 9.0 keV (Kβ), along with Fe peaks at ~ 6.3 keV (Kα) and ~ 7.1 keV (Kβ), confirm the incorporation of these elements. The O Kα peak (~0.5 keV) indicates oxygen's presence in the ferrite structure. A carbon (C Kα) peak (~0.3 keV) is also observed, likely originating from Chlorella vulgaris residues in the green synthesis or from carbon coating used during SEM-EDS. Additionally, minor traces of bromine (Br), chlorine (Cl), and sulfur (S) are detected, which may stem from organic residues or precursor materials. However, their low intensity suggests minimal impact on the final product's purity. Literature on $CuFe_2O_4$ NPs synthesized reports similar elemental compositions, reinforcing the reliability of this green synthesis method [45–47]. The strong Cu, Fe, and O signals confirm the expected stoichiometric composition of $CuFe_2O_4$ without significant impurity phases.

3.3. Wettability of copper ferrite nanofluids

Wettability is a key parameter used to characterize the chemical and physical properties of a surface and is typically determined by measuring the contact angle of a liquid droplet on the surface [48]. The interaction between a solid surface and a fluid is influenced by factors such as surface energy, surface texture, and chemical composition [49]. Additionally, the fluid's properties, such as surface tension, can also impact wettability measurements.

In this study, the contact angles of $CuFe_2O_4$-based nanofluids at concentrations of 0.1 wt%, 0.5 wt%, and 1 wt% were measured on two types of substrates: (i) Aluminum, a widely used material in heat exchangers due to its high thermal conductivity, lightweight nature, oxidation resistance, and cost-effectiveness compared to copper; (ii) PDMS, as the heat exchanger later used to evaluate the heat transfer capacity of the nanofluids is made from this material. To assess the significance of variations in contact angle under different conditions relative to the control group (water-based fluid without NPs), a Dunnett multiple comparison test was conducted (for detailed information, see Table S1 in supplementary material).

The contact angles of $CuFe_2O_4$-based nanofluids at concentrations of 0.1 wt%, 0.5 wt%, and 1 wt% on both substrates are shown in Fig. 7**.** On the aluminum substrate, a significant increase in the contact angle was observed at the lowest concentration (0.1 wt%) compared to the control (water). However, no significant changes were noted at higher concentrations. This behavior may indicate better dispersion of $CuFe_2O_4$ NPs at lower concentrations, which optimally covers the surface and alters the surface energy of the aluminum substrate, resulting in a higher contact angle. At higher NP concentrations, increased particle interactions and aggregation reduce their effective interaction with the substrate, diminishing their influence on surface energy and contact angle. These findings suggest that at higher concentrations, the wettability behavior of the nanofluid becomes similar to that of water.

For the PDMS substrate, a generalized increase in contact angles compared to aluminum was observed. This result is expected, as PDMS is a silicone-based polymer with inherently low surface energy, making it

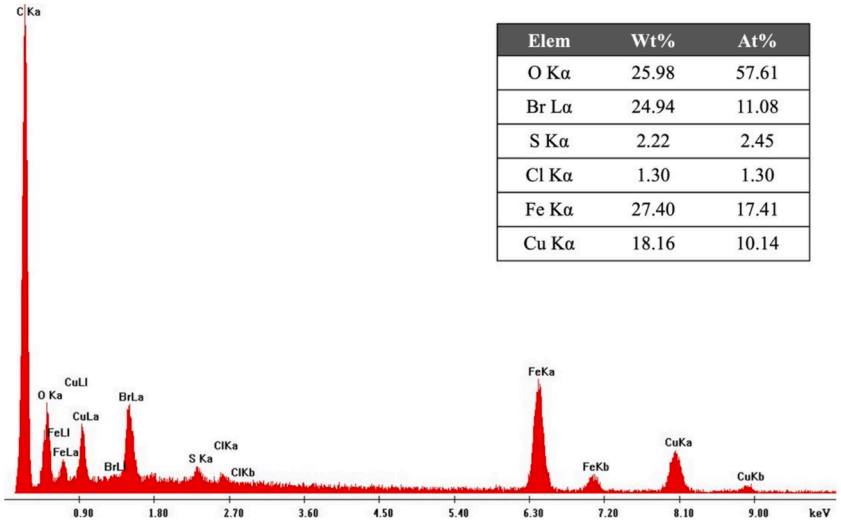

Elem	Wt%	At%
O Kα	25.98	57.61
Br Lα	24.94	11.08
S Kα	2.22	2.45
Cl Kα	1.30	1.30
Fe Kα	27.40	17.41
Cu Kα	18.16	10.14

Fig. 6. EDS spectrum of the green synthesized $CuFe_2O_4$ NPs using *Chlorella vulgaris* aqueous extract.

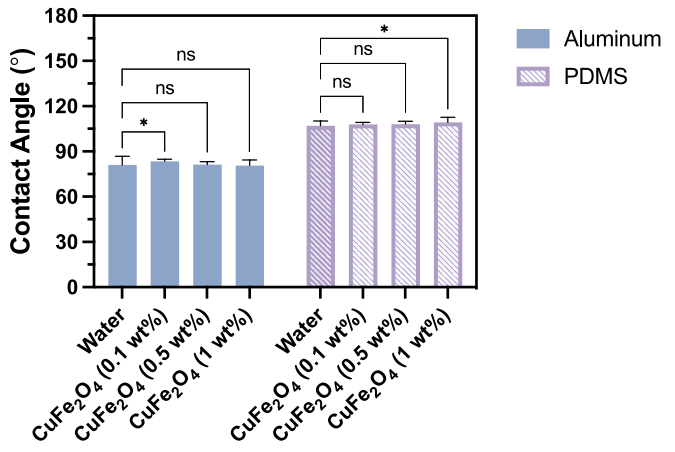

Fig. 7. Contact angles of $CuFe_2O_4$ NPs-based nanofluids at 0.1 wt%, 0.5 wt%, and 1 wt% on aluminum and PDMS substrates. Data represent the mean contact angle values ± SD of three independent experiments. Error bars indicate the standard deviation of three measurements. Multiple comparisons with the Dunnett test. *p < 0.05; **p < 0.01; ***p < 0.001; ****p < 0.0001, ns: not significant; by ANOVA followed by Dunnett's post-test.

more hydrophobic than aluminum. Notably, only the highest concentration of $CuFe_2O_4$ NPs (1 wt%) caused a significant change in contact angle compared to the control. At lower concentrations, the minimal surface coverage provided by the dispersed NPs is insufficient to alter the surface energy of PDMS. In contrast, a higher NP density at 1 wt% overcomes the hydrophobic nature of PDMS, leading to a measurable change in the contact angle relative to water. The observed increase in contact angle with increasing NP concentration deviates from the commonly reported trend in nanofluid wettability research, where a decrease in contact angle is typically observed [50]. This discrepancy highlights the complex interplay of factors governing nanofluid wettability. While nanoparticle concentration plays a significant role, parameters such as nanoparticle size and shape, along with their interaction with the substrate, can also influence the contact angle. In our study, the presence of biomolecules bound to the nanoparticles adds another layer of complexity. These biomolecules can alter the aggregation behavior of the nanoparticles and modify their electrostatic properties, providing plausible explanations for the observed increase in contact angle.

It is important to note that wettability is not typically a critical parameter in heat transfer for closed, single-phase systems and is generally disregarded regardless of the coil material [30,51,52]. Therefore, while significant variations in wettability were observed between aluminum and PDMS substrates, these differences are unlikely to impact heat exchange performance, as they would in two-phase systems [53].

However, wettability becomes a critical parameter in two-phase systems, such as heat pipes. In these systems, a smaller contact angle increases the contact area between the fluid and the surface, enhancing the fluid's ability to transfer heat efficiently from the surface to the fluid [54]. In heat pipes with a wick structure, a more wetting fluid is particularly desirable due to the capillary effect. A lower contact angle increases capillary pressure, which improves the fluid's flow rate and the distance it can travel, thereby enhancing the overall heat transfer capacity [55]. On the other hand, increasing the contact angle can lead to the formation of smaller droplets in the condensers, increasing the detachment speed and, consequently, improving the thermal performance of two-phase heat exchangers [56].

3.4. Viscosity of copper ferrite nanofluids

Adding NPs to a base fluid can significantly alter its thermophysical properties. The volume concentration of nanofluids is a key factor that directly influences both thermal properties and viscosity. Several studies have shown that increasing the NP's weight percentage leads to higher viscosity and thermal conductivity [57–60]. However, this increase in viscosity can cause greater pressure losses, thereby raising the pumping power required [61]. Therefore, achieving a balance between enhanced thermal conductivity and manageable viscosity is crucial to avoid compromising the overall performance of nanofluids.

In this study, the viscosity of the nanofluids was analyzed as a function of shear rate and NPs concentration (Fig. 8). The viscosity results were compared to those of the base fluid (water) without NPs.

An increase in viscosity was observed for all nanofluids compared to water, as expected since the presence of NPs introduces internal friction and resistance to flow. However, the viscosity increase was not directly proportional to NP concentration. Notably, nanofluids with a 0.1 wt% NP concentration exhibited a higher viscosity (~1.1 mPa·s) compared to those with 0.5 wt% and 1 wt% concentrations (1 mPa·s) although almost always within the margin of imprecision. This behavior parallels the trends observed in the wettability assays, where higher NP concentrations appear to promote greater particle aggregation. Aggregation reduces the effective surface area of NPs available for interaction with the fluid, thereby influencing the stability and rheological behavior of the nanofluid. Additionally, the viscosity values for nanofluids containing 0.1 wt% and 0.5 wt% NPs were nearly identical, suggesting that a saturation point may have been reached. Beyond this point, further increases in NP concentration do not significantly alter the viscosity of the nanofluid.

The results are consistent with those found by Aguilar *et al.* [62] that added $CuFe_2O_4$ NPs to Dowtherm A using oleic acid as a surfactant, where there was an unequivocal increase in viscosity upon addition of nanoparticles, but which is not reflected in significant changes with increasing concentration. Yakymovych *et al.* [63] conducted viscosity tests on nanofluids with iron nanoparticles and observed an increase in viscosity from the lowest concentration tested (0.5 wt%) without significant further increase up to the maximum tested concentration of 2.0 wt%.

3.5. Thermal conductivity of copper ferrite nanofluids

The thermal conductivity of nanofluids is strongly influenced by both the type of NPs used and the properties of the base fluid in which they are dispersed [64]. Several studies have highlighted the role of NP concentration on thermal conductivity, often demonstrating non-linear

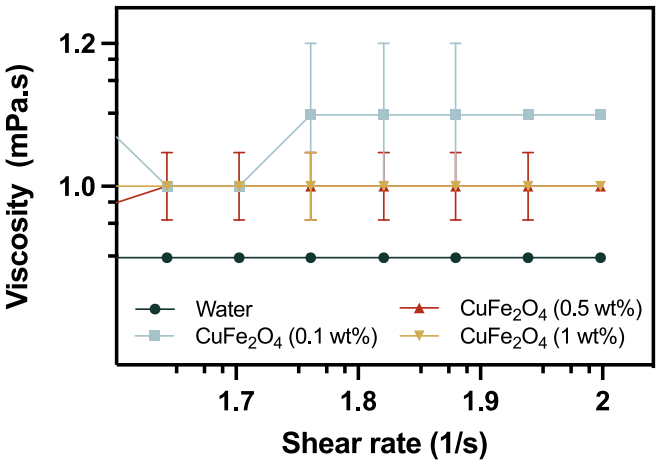

Fig. 8. Viscosities of water and nanofluids containing $CuFe_2O_4$ NPs at 0.1 wt%, 0.5 wt%, and 1 wt%, using water as a base fluid. Data represent the mean viscosities values ± SD of three independent experiments. Error bars indicate the standard deviation of three measurements.

effects at varying concentrations [65–67]. Fig. 9 presents the thermal conductivity values (W/mK) for $CuFe_2O_4$-based nanofluids at concentrations of 0.1 wt%, 0.5 wt%, and 1 wt%, compared to water. A Dunnett multiple comparison test was conducted to evaluate the statistical significance of the variations observed under different conditions relative to water (for detailed information, see Table S2 in supplementary material).

The results revealed a general increase in thermal conductivity with rising NP concentrations in the nanofluid. However, a statistically significant enhancement over water was only observed at a concentration of 1 wt%, corresponding to a 4.8 % increase in thermal conductivity. Similar trends have been reported in studies using green-synthesized metallic NPs. For instance, Sa and Nath [68] demonstrated improved thermal conductivity in water-based nanofluids with Fe_3O_4 NPs synthesized using *Aloe barbadensis* leaf extract. Nonetheless, the enhancement achieved in this study is lower compared to the 27 % increase observed by Omiddezyani *et al.* [19], who investigated nanofluids containing $CoFe_2O_4$/rGO NPs synthesized using gallic acid at a concentration of 0.9 wt%. These findings underscore the potential of green synthesis in developing nanofluids, though the extent of thermal conductivity enhancement varies with NP composition and synthesis method.

3.6. Heat exchanger of copper ferrite nanofluids (serpentine)

Based on the results obtained for the nanofluids' thermal conductivity, only the concentration with the best performance (1 wt%) was selected for further evaluation. A key parameter analyzed was the temperature difference between the inlet and outlet of the nanofluid in the serpentine system (Fig. 10). A Šídák's multiple comparison test was conducted to evaluate the statistical significance of the variations observed between water and $CuFe_2O_4$ 1 wt% nanofluid at 5 ml/min, 10 ml/min and 15 ml/min flow rates (for detailed information, see Table S3 in supplementary material).

The results show that the nanofluid exhibits a more significant temperature variation than water, with approximately 0.6 °C at a volumetric flow rate of 5 mL/min and ~ 0.5 °C at 10 and 15 mL/min.

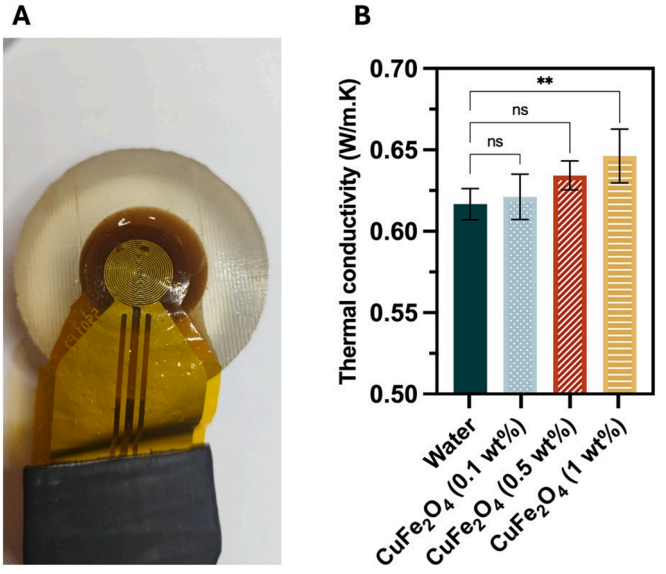

Fig. 9. (A) Experimental apparatus for thermal conductivity measurement and (B) thermal conductivity of water and nanofluids containing $CuFe_2O_4$ NPs at 0.1 wt%, 0.5 wt%, and 1 wt%. Data represent the mean and show the mean thermal conductivity values ± SD of three independent experiments. Error bars indicate the standard deviation of three measurements. Multiple comparisons with the Dunnett test.*$p < 0.05$; **$p < 0.01$; ***$p < 0.001$; ****$p < 0.0001$, ns: not significant; by ANOVA followed by Dunnett's post-test.

These findings align with previous studies on green nanofluids, which also reported enhanced heat transfer performance and greater temperature variation compared to the base fluid [69,70]. The results are in agreement with those previously obtained [71], where iron oxide NPs synthesized with aqueous extract of *Chlorella vulgaris* exhibited a significantly higher temperature variation than the base fluid at all tested flow rates. Since heat absorption is closely linked to temperature variation, the nanofluid is expected to demonstrate higher heat absorption capacity. Additionally, as the nanofluid's temperature rises, its potential for use in applications such as residential and commercial heating or industrial processes increases. The results indicate that even a slight improvement in the fluid's thermal properties can lead to significant temperature differences in practical applications. Furthermore, the enhancement of the nanofluid's thermal conductivity is more pronounced with increased temperature [68].

Other factors related to nanofluids, such as particle size, shape, alignment, and hydrogen bonding, can interact in ways that often exceed predictions, yielding even better results than expected [72]. Fig. 11 illustrates the nanofluid's heat storage rate, which is higher than that of water, and it increases with higher volumetric flow rates. A Šídák's multiple comparison test was conducted to evaluate the statistical significance of the variations observed between water and $CuFe_2O_4$ 1 wt% nanofluid at 5 ml/min, 10 ml/min and 15 ml/min flow rates (for detailed information, see Table S4 in supplementary material). This analysis revealed that the heat performance enhancement of the $CuFe_2O_4$ nanofluid (1 wt%) was statistically significant only at a volumetric flow rate of 15 mL/min. This significant difference in performance only at the highest flow rate tested may be related to the tendency of the NPs to remain better dispersed when there is greater fluid agitation.

This behavior underscores the importance of nanofluids in heat transfer applications, demonstrating their superior cooling capacity. On average, the heat stored of the nanofluid is 38 % to 95 % higher than that of water, following Eq. (2).

However, upon closer analysis, the behavior of water deviates from expectations. Typically, an increase in volumetric flow rate results in a higher deviate [73], but slight deviations in this trend were observed. These deviations can be attributed to factors such as thermocouple inaccuracies and the low power of the heat source, which was affected by the limited amount of nanofluid, making the system more susceptible to random fluctuations. The observed trend of reduced power transfer with increasing volumetric flow rates in the water results may reflect potential anomalies. It is also important to note that considering the uncertainties, the power removal in nanofluid results could be less effective than that of water, though its ability to increase temperature is more significant despite these uncertainties.

4. Conclusions

This study successfully demonstrated the green synthesis of copper ferrite nanoparticles ($CuFe_2O_4$ NPs) using the aqueous extract of *Chlorella vulgaris*, providing an eco-friendly and sustainable approach to NPs production. The synthesis was monitored through UV–vis spectroscopy, which revealed a blue shift in absorption peaks from 380 nm to 350 nm over 4 h of reaction, indicating progressive nanoparticle formation, nucleation, and growth. The band gap energy decreased from 2 eV to 1.83 eV, corresponding to increased particle size and enhanced crystallinity. Morphological analysis using scanning electron microscopy confirmed uniform particle sizes, with a mean size of 130 nm and a narrow size distribution. The EDS results confirmed their elemental composition, with strong signals corresponding to Cu, Fe, and O, verifying the formation of the expected spinel ferrite structure. Minor traces of Br, Cl, and S were observed, likely due to residual organic compounds from the green synthesis route, but their low intensity suggests minimal influence on the final product's properties.

The $CuFe_2O_4$ NPs were dispersed in water at concentrations of 0.1 wt

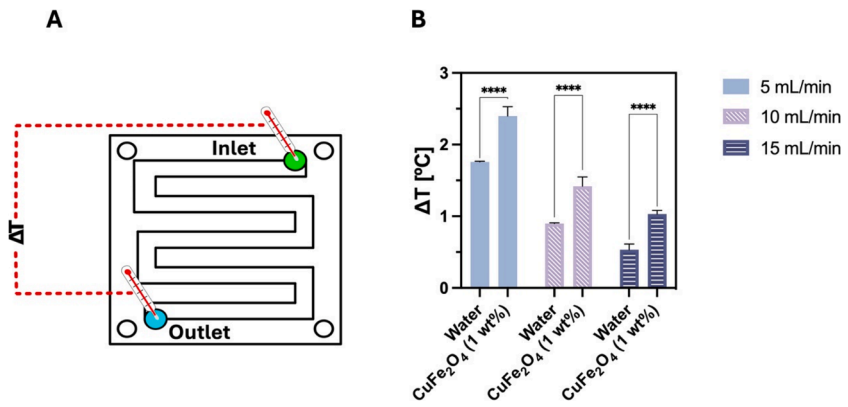

Fig. 10. (A) Schematic representation of the temperature variation measurement between the inlet and outlet, and (B) experimental temperature variation between the inlet and outlet of the serpentine channel for water and $CuFe_2O_4$ 1 wt% nanofluid at 5 ml/min, 10 ml/min and 15 ml/min flow rates. Data represent the mean ± standard deviation of three independent experiments. Error bars indicate the standard deviation of three measurements. Multiple comparisons with using Šídák's test. *p < 0.05; **p < 0.01; ***p < 0.001; ****p < 0.0001, ns: not significant; by ANOVA followed by Šídák's post-test.

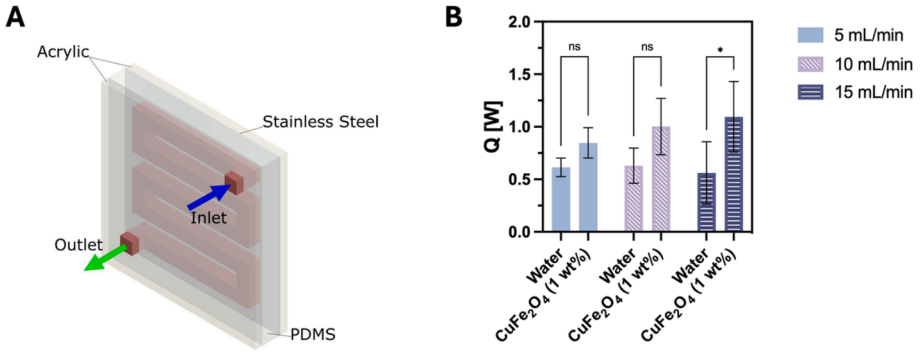

Fig. 11. (A) Schematic representation of the PDMS-based heat exchanger (serpentine) and (B) heat storage rate as a function of the volumetric flow rate of water and $CuFe_2O_4$ (1 wt%) nanofluid with the respective standard deviation. Data represent the mean ± standard deviation of three independent experiments. Error bars indicate the standard deviation of three measurements. Multiple comparisons with using Šídák's test. *p < 0.05; **p < 0.01; ***p < 0.001; ****p < 0.0001, ns: not significant; by ANOVA followed by Šídák's post-test.

%, 0.5 wt%, and 1 wt% to create nanofluids, and their properties were comprehensively characterized. Wettability results highlighted substrate-specific behavior. On aluminum, a significant increase in contact angle at 0.1 wt% (compared to water) suggested optimal NPs dispersion, while at higher concentrations, NPs aggregation reduced their surface interaction. On the more hydrophobic PDMS substrate, only the 1 wt% nanofluid significantly altered the contact angle, underscoring the concentration-dependent interaction of nanoparticles with surfaces. These variations, however, are unlikely to impact heat transfer performance in single-phase systems but may influence two-phase systems.

Viscosity measurements revealed a slight increase across all nanofluids compared to water, with the 0.1 wt% concentration showing the highest viscosity (~1.1 mPa·s). This behavior suggests that lower concentrations may exhibit better dispersion, while higher concentrations lead to aggregation, limiting further viscosity changes. Importantly, the viscosities remained within manageable limits, ensuring minimal impact on pumping power requirements and practical applicability.

Thermal conductivity testing showed that the nanofluids improved thermal performance, with the 1 wt% nanofluid achieving a 4.8 % enhancement compared to water. This improvement translated into substantial heat transfer efficiency gains during experiments using a serpentine heat exchanger. The 1 wt% nanofluid demonstrated remarkable heat absorption increases, ranging from 38 % to 95 %, depending on the volumetric flow rate (5–15 mL/min). These results highlight the nanofluid's capacity to outperform water, particularly under higher flow rates, where its enhanced thermal properties significantly improve heat removal.

In summary, the $CuFe_2O_4$-based nanofluids synthesized via a green synthesis demonstrated substantial improvements in heat transfer properties while maintaining practical wettability and viscosity features. These findings emphasize the potential of green-synthesized nanofluids as sustainable, high-performance alternatives for thermal management applications in both monophasic and biphasic systems. The results also encourage further exploration of bio-synthesized nanoparticles for a wide range of industrial and energy applications.

CRediT authorship contribution statement

Beatriz Cardoso: Writing – original draft, Supervision, Software, Methodology, Formal analysis, Conceptualization. **Glauco Nobrega:** Supervision, Methodology, Investigation. **Mariana Machado:** Writing – original draft, Investigation, Formal analysis, Data curation. **Rui A. Lima:** Writing – review & editing, Supervision, Resources.

Declaration of competing interest

The authors declare that they have no known competing financial interests or personal relationships that could have appeared to influence the work reported in this paper.

Acknowledgments

The authors acknowledge the partial financial support of the projects

2022.06207.PTDC (https://doi.org/10.54499/2022.06207.PTDC) through national funds (OE), within the scope of the Scientific Research and Technological Development Projects (IC&DT) program in all scientific domains (PTDC), through the Foundation for Science and Technology, I.P. (FCT, I.P). The authors acknowledge the partial financial support within the R&D Units Project Scope: : UIDB/04077/2020, UIDP/04077/2020 (UID/4077: Mechanical Engineering and Resource Sustainability Center (MEtRICs)), UIDB/00532/2020, and LA/P/0045/2020 (ALiCE). FCT/MCTES (PIDDAC) to Centro de Investigação de Montanha (CIMO) (UIDB/00690/2020 and UIDP/00690/2020) and SusTEC (LA/P/0007/2020). Glauco Nobrega was supported by the doctoral grant PRT/BD/153088/2021, financed by the Portuguese Foundation for Science and Technology (FCT), and with funds from MCTES/República Portuguesa, under the MIT Portugal Program. The authors would like to thank Marta Fernanda and Professor Andrea Zille from 2C2T—Centre for Textile Science and Technology (University of Minho), for their support with the spectrophotometer and the SEM images.

Appendix A. Supplementary data

Supplementary data to this article can be found online at https://doi.org/10.1016/j.molliq.2025.127498.

Data availability

Data will be made available on request.

References

[1] L. Godson, B. Raja, D.M. Lal, S. Wongwises, Enhancement of heat transfer using nanofluids—an overview, Renew. Sustain. Energy Rev. 14 (2010) 629–641.
[2] N. El Messaoudi, Z. Ciğeroğlu, Z.M. Şenol, E.S. Kazan-Kaya, Y. Fernine, S. Gubernat, Z. Lopicic, Green synthesis of CuFe2O4 nanoparticles from bioresource extracts and their applications in different areas: a review, Biomass Convers. Biorefin. (2024) 1–22.
[3] W.H. Azmi, K.V. Sharma, R. Mamat, G. Najafi, M.S. Mohamad, The enhancement of effective thermal conductivity and effective dynamic viscosity of nanofluids–a review, Renew. Sustain. Energy Rev. 53 (2016) 1046–1058.
[4] M.U. Sajid, H.M. Ali, Recent advances in application of nanofluids in heat transfer devices: a critical review, Renew. Sustain. Energy Rev. 103 (2019) 556–592.
[5] M.H. Ahmadi, A. Mirlohi, M.A. Nazari, R. Ghasempour, A review of thermal conductivity of various nanofluids, J. Mol. Liq. 265 (2018) 181–188.
[6] M.S. Chowdhury, M.Z. Abedin, M.W. Rahman, Nanofluids in nuclear power plants, A Comprehensive Review (2023).
[7] J. Patel, A. Soni, D.P. Barai, B.A. Bhanvase, A minireview on nanofluids for automotive applications: Current status and future perspectives, Appl. Therm. Eng. 219 (2023) 119428.
[8] G. Nobrega, B. Cardoso, R. Souza, J. Pereira, P. Pontes, S.O. Catarino, D. Pinho, R. Lima, A. Moita, A Review of Novel Heat Transfer Materials and Fluids for Aerospace Applications, Aerospace 11 (2024) 275.
[9] G. Nobrega, I.S. Afonso, B. Cardoso, R.R. de Souza, A. Moita, J.E. Ribeiro, R. A. Lima, Exploring heat exchange in space: Recent advances in two-phase fluid experiments in microgravity, Therm. Sci. Eng. Prog. 103025 (2024).
[10] H. Kaya, E. Alp, Experimental investigation of effect of iron oxide nanofluids with different morphology on heat transfer of multiple impinging jets, Exp. Heat Transfer 36 (2023) 719–733.
[11] A. Sumithra, B.R. Kumar, R. Sivaraj, H.F. Öztop, Thermal analysis of magnetic Iron-Oxide nanoparticle with combination of Water and Ethylene Glycol passes through a partially heated permeable square enclosure, Journal of Taibah University for Science 17 (2023) 2257366.
[12] S.A. Kadhim, A.H. Askar, A.A.M. Saleh, An enhancement of double pipe heat exchanger performance at a constant wall temperature using a nanofluid of iron oxide and refrigerant vapor, J. Therm. Eng. 10 (2024) 78–87.
[13] A. Bhattad, B.N. Rao, V. Atgur, N.R. Banapurmath, A.M. Sajjan, C. Vadlamudi, S. Krishnappa, T. Yunus Khan, N.H. Ayachit, Studies on evaluation of the thermal conductivity of alumina titania hybrid suspension nanofluids for enhanced heat transfer applications, ACS Omega 8 (2023) 24176–24184.
[14] A.B. Mahfouz, A. Ali, M. Mubashir, A.S. Hanbazazah, M. Alsaady, P.L. Show, Optimization of viscosity of titania nanotubes ethylene glycol/water-based nanofluids using response surface methodology, Fuel 347 (2023) 128334.
[15] D. Yogaraj, S. Deepak, G.J. Rakshgan, P. Dwarakesh, R. Vishwakarma, P.K. Kujur, Y.A. Rao, Thermal performance analysis of a counter-flow double-pipe heat exchanger using titanium oxide and zinc oxide nanofluids, Mater. Today Proc. (2023).
[16] M. Arun, Experimental investigation on energy and exergy analysis of solar water heating system using zinc oxide-based Nanofluid, Arab. J. Sci. Eng. 48 (2023) 3977–3988.
[17] P.K. Kanti, P. Sharma, K. Sharma, M. Maiya, The effect of pH on stability and thermal performance of graphene oxide and copper oxide hybrid nanofluids for heat transfer applications: application of novel machine learning technique, Journal of Energy Chemistry 82 (2023) 359–374.
[18] A.S.M. Aljaloud, K. Smida, H.F.M. Ameen, M. Albedah, I. Tlili, Investigation of phase change and heat transfer in water/copper oxide nanofluid enclosed in a cylindrical tank with porous medium: a molecular dynamics approach, Eng. Anal. Bound. Elem. 146 (2023) 284–291.
[19] S. Omiddezyani, S. Gharehkhani, V. Yousefi-Asli, I. Khazaee, M. Ashjaee, R. Nayebi, F. Shemirani, E. Houshfar, Experimental investigation on thermo-physical properties and heat transfer characteristics of green synthesized highly stable CoFe2O4/rGO nanofluid, Colloids Surf. A Physicochem. Eng. Asp 610 (2021) 125923.
[20] N. Kahzad, A. Salehzadeh, Green synthesis of CuFe2O4@ Ag nanocomposite using the Chlorella vulgaris and evaluation of its effect on the expression of norA efflux pump gene among Staphylococcus aureus strains, Biol. Trace Elem. Res. 198 (2020) 359–370.
[21] A.K. Sidhu, N. Verma, P. Kaushal, Role of biogenic capping agents in the synthesis of metallic nanoparticles and evaluation of their therapeutic potential, Front. Nanotechnol. 3 (2022) 801620.
[22] A.H. Cahyana, A.R. Liandi, Y. Yulizar, Y. Romdoni, T.P. Wendari, Green synthesis of CuFe2O4 nanoparticles mediated by Morus alba L. leaf extract: crystal structure, grain morphology, particle size, magnetic and catalytic properties in Mannich reaction, Ceram. Int. 47 (2021) 21373–21380.
[23] S. Ying, Z. Guan, P.C. Ofoegbu, P. Clubb, C. Rico, F. He, J. Hong, Green synthesis of nanoparticles: current developments and limitations, Environ. Technol. Innov. 26 (2022) 102336.
[24] P. Khanna, A. Kaur, D. Goyal, Algae-based metallic nanoparticles: synthesis, characterization and applications, J. Microbiol. Methods 163 (2019) 105656.
[25] D. Sharma, S. Kanchi, K. Bisetty, Biogenic synthesis of nanoparticles: a review, Arab. J. Chem. 12 (2019) 3576–3600.
[26] K. Pal, S. Chakroborty, N. Nath, Limitations of nanomaterials insights in green chemistry sustainable route: review on novel applications, Green Process. Synth, 11 (2022) 951–964.
[27] C.Y. Rahimzadeh, A.A. Barzinjy, A.S. Mohammed, S.M. Hamad, Green synthesis of SiO2 nanoparticles from Rhus coriaria L. extract: comparison with chemically synthesized SiO2 nanoparticles, PLoS One 17 (2022) e0268184.
[28] F. Arsiya, M.H. Sayadi, S. Sobhani, Green synthesis of palladium nanoparticles using Chlorella vulgaris, Mater. Lett. 186 (2017) 113–115.
[29] R. Souza, F.S. Barbosa, G. Nobrega, E. Cardoso, J. Teixeira, A. Moita, R. Lima, An innovative PDMS cell to improve the thermal conductivity measurements of nanofluids, Therm. Sci. Eng. Prog. 42 (2023) 101926.
[30] R. Souza, F.S. Barbosa, G. Nobrega, E. Cardoso, J. Teixeira, A. Moita, R. Lima, Experimental study of an innovative elastomer-based heat exchanger, Case Stud. Therm. Eng. 49 (2023) 103365.
[31] C. Selvam, D. Mohan Lal, S. Harish, Thermal conductivity and specific heat capacity of water–ethylene glycol mixture-based nanofluids with graphene nanoplatelets, J. Therm. Anal. Calorim. 129 (2017) 947–955.
[32] D. Kalantari, M. Tafakhori, M. Ghanbari, P. Biparva, S. Peyghambarzadeh, Intensification of thermal efficiency of a cross-flow heat exchanger under turbulent flow conditions using CuFe2O4/water nanofluid, Int. J. Therm. Sci. 185 (2023) 108107.
[33] Z. Ye, Z. Deng, L. Zhang, J. Chen, G. Wang, Z. Wu, The structure of copper ferrite prepared by five methods and its catalytic activity on lignin oxidative degradation, Mater. Res. Express 7 (2020) 035007.
[34] J. Turkevich, P.C. Stevenson, J. Hillier, A study of the nucleation and growth processes in the synthesis of colloidal gold, Discuss. Faraday Soc. 11 (1951) 55–75.
[35] R. Javed, M. Zia, S. Naz, S.O. Aisida, N.U. Ain, Q. Ao, Role of capping agents in the application of nanoparticles in biomedicine and environmental remediation: recent trends and future prospects, J Nanobiotechnol. 18 (2020) 1–15.
[36] S. Link, M.A. El-Sayed, Shape and size dependence of radiative, non-radiative and photothermal properties of gold nanocrystals, Int. Rev. Phys. Chem. 19 (2000) 409–453.
[37] L.E. Brus, Electron–electron and electron-hole interactions in small semiconductor crystallites: the size dependence of the lowest excited electronic state, J. Chem. Phys. 80 (1984) 4403–4409.
[38] R.J. Fernandes, B.D. Cardoso, A.R.O. Rodrigues, A. Pires, A.M. Pereira, J.P. Araújo, L. Pereira, P.J. Coutinho, Zinc/magnesium ferrite nanoparticles functionalized with silver for optimized photocatalytic removal of malachite green, Materials 17 (2024) 3158.
[39] H. Zhang, J.F. Banfield, Understanding polymorphic phase transformation behavior during growth of nanocrystalline aggregates: insights from TiO2, J. Phys. Chem. B 104 (2000) 3481–3487.
[40] B.D. Cardoso, A.R.O. Rodrigues, M. Bañobre-López, B.G. Almeida, C.O. Amorim, V. S. Amaral, P.J. Coutinho, E.M. Castanheira, Magnetoliposomes based on shape anisotropic calcium/magnesium ferrite nanoparticles as nanocarriers for doxorubicin, Pharmaceutics 13 (2021) 1248.
[41] M. Sravanthi, D. Muni Kumar, B. Usha, M. Ravichandra, M. Mahendra Rao, K. Hemalatha, M. Ravichandra, Biological synthesis and characterization of copper oxide nanoparticles using Antigonon leptopus leaf extract and their antibacterial activity, Int. J. Adv. Res 4 (2016) 589–602.
[42] M. Khatami, K. Ebrahimi, N. Galehdar, M.N. Moradi, A. Moayyedkazemi, Green synthesis and characterization of copper nanoparticles and their effects on liver

function and hematological parameters in mice, Turkish J. Pharmaceut. Sci. 17 (2020) 412.
[43] Z. Alhalili, Green synthesis of copper oxide nanoparticles CuO NPs from Eucalyptus globoulus leaf extract: adsorption and design of experiments. Arab. J. Chem. 15 (5): 103739, Alsamhary, K, (2022) 3326-3337.
[44] I.S. Afonso, B. Cardoso, G. Nobrega, G. Minas, J.E. Ribeiro, R.A. Lima, Green synthesis of nanoparticles from olive oil waste for environmental and health applications: a review, J. Environ. Chem. Eng. 114022 (2024).
[45] A.B. Ghumare, M.L. Mane, S.E. Shirsath, K. Lohar, Role of pH and sintering temperature on the properties of tetragonal–cubic phases composed copper ferrite nanoparticles, J. Inorg. Organomet. Polym Mater. 28 (2018) 2612–2619.
[46] P.A. Udhaya, A. Ahmad, M. Meena, M.A.J. Queen, M. Aravind, P. Velusamy, T. M. Almutairi, A.A. Mohammed, S. Ali, Copper Ferrite nanoparticles synthesised using a novel green synthesis route: Structural development and photocatalytic activity, J. Mol. Struct. 1277 (2023) 134807.
[47] F. Germaninezhad, R. Hosseinzadeh, M. Tajbakhsh, A. Beitollahi, Copper ferrite nanoparticles: an effective and recoverable nanomagnetic catalyst for the synthesis of N, N′, N ″-trisubstituted guanidines from the addition reaction of anilines to carbodiimide, Micro Nano Lett. 15 (2020) 359–364.
[48] L. Chen, E. Bonaccurso, Electrowetting—from statics to dynamics, Adv. Colloid Interface Sci. (2013).
[49] M.A. Henderson, The interaction of water with solid surfaces: fundamental aspects revisited, Surf. Sci. Rep. 46 (2002) 1–308.
[50] J. Chinnam, D. Das, R. Vajjha, J. Satti, Measurements of the contact angle of nanofluids and development of a new correlation, Int. Commun. Heat Mass Transfer 62 (2015) 1–12.
[51] S. Nada, R. El-Zoheiry, M. Elsharnoby, O. Osman, Experimental investigation of hydrothermal characteristics of data center servers' liquid cooling system for different flow configurations and geometric conditions, Case Stud. Therm. Eng. 27 (2021) 101276.
[52] A.M. Bassam, K. Sopian, A. Ibrahim, A.B. Al-Aasam, M. Dayer, Experimental analysis of photovoltaic thermal collector (PVT) with nano PCM and micro-fins tube counterclockwise twisted tape nanofluid, Case Stud. Therm. Eng. 45 (2023) 102883.
[53] E. Freitas, P. Pontes, R. Cautela, V. Bahadur, J. Miranda, A.P. Ribeiro, R.R. Souza, J.D. Oliveira, J.B. Copetti, R. Lima, Pool boiling of nanofluids on biphilic surfaces: an experimental and numerical study, Nanomaterials 11 (2021) 125.
[54] X. Yin, C. Hu, M. Bai, J. Lv, Molecular dynamic simulation of rapid boiling of nanofluids on different wetting surfaces with depositional nanoparticles, Int. J. Multiph. Flow 115 (2019) 9–18.
[55] A.M. Sebayang, A.P. Tetuko, L.F. Nurdiyansah, N.S. Asri, E.A. Setiadi, P. Sebayang, Wick parameters (particle size, porosity and contact angle) and performances of a U-shaped heat pipe: experimental, analytical and numerical, Aust. J. Mech. Eng. 22 (2024) 552–565.
[56] B. Qi, J. Wei, L. Zhang, H. Xu, A fractal dropwise condensation heat transfer model including the effects of contact angle and drop size distribution, Int. J. Heat Mass Transf. 83 (2015) 259–272.
[57] T.-B. Chang, S.-C. Syu, Y.-K. Yang, Effects of particle volume fraction on spray heat transfer performance of Al2O3–water nanofluid, Int. J. Heat Mass Transf. 55 (2012) 1014–1021.
[58] L. Chen, H. Xie, Y. Li, W. Yu, Nanofluids containing carbon nanotubes treated by mechanochemical reaction, Thermochim. Acta 477 (2008) 21–24.
[59] M. Kole, T. Dey, Viscosity of alumina nanoparticles dispersed in car engine coolant, Exp. Therm Fluid Sci. 34 (2010) 677–683.
[60] A. Turgut, I. Tavman, M. Chirtoc, H. Schuchmann, C. Sauter, S. Tavman, Thermal conductivity and viscosity measurements of water-based TiO2 nanofluids, Int. J. Thermophys. 30 (2009) 1213–1226.
[61] S. Murshed, K. Leong, C. Yang, Investigations of thermal conductivity and viscosity of nanofluids, Int. J. Therm. Sci. 47 (2008) 560–568.
[62] T. Aguilar, I. Carrillo-Berdugo, R. Alcantara, J. Navas, Enhanced thermophysical properties in spinel CuFe2O4-based nanofluids for concentrated solar power, Int. J. Energy Res. 46 (2022) 4908–4918.
[63] A. Yakymovych, I. Wodak, G. Khatibi, Hybrid solder joints: viscosity studies of the nanocomposite flux with Fe nanoparticle additions, Metals 15 (2025) 93.
[64] A. Hemmati-Sarapardeh, A. Varamesh, M.N. Amar, M.M. Husein, M. Dong, On the evaluation of thermal conductivity of nanofluids using advanced intelligent models, Int. Commun. Heat Mass Transfer 118 (2020) 104825.
[65] L.S. Sundar, M.J. Hortiguela, M.K. Singh, A.C. Sousa, Thermal conductivity and viscosity of water based nanodiamond (ND) nanofluids: an experimental study, Int. Commun. Heat Mass Transfer 76 (2016) 245–255.
[66] P.K. Das, A.K. Mallik, R. Ganguly, A.K. Santra, Synthesis and characterization of TiO2–water nanofluids with different surfactants, Int. Commun. Heat Mass Transfer 75 (2016) 341–348.
[67] S. Iqbal, C. Raj, J. Michael, A. Irfan, A comparative investigation of Al2O3/H2O, SiO2/H2O and ZrO2/H2O nanofluid for heat transfer applications, Digest J. Nanomater. Biostruct. (DJNB) 12 (2017).
[68] J. Sa, G. Nath, Study on Thermoacoustic Properties of Ultrasonic Assisted Green Synthesized Fe3O4 Nanofluid.
[69] S.K. Shanmugam, A. Arivendan, S. Govindan Selvamani, T. Dheivasigamani, T. K. Sundaresan, S. Ali, Characterization and heat transfer assessment of CuO-based nanofluid prepared through a green synthesis process, Ceramics 6 (2023) 1926–1936.
[70] N.C. Maji, J. Chakraborty, Gram-scale green synthesis of copper nanowire powder for nanofluid applications, ACS Sustain. Chem. Eng. 7 (2019) 12376–12388.
[71] G. Nobrega, R. Souza, B. Cardoso, I. Afonso, J. Pereira, E. Cardoso, A. Moita, J. Ribeiro, R. Lima, Experimental evaluation of green nanofluids in heat exchanger made oF PDMS, Therm. Sci. Eng. Prog. 55 (2024) 102978.
[72] H. Younes, M. Mao, S.S. Murshed, D. Lou, H. Hong, G. Peterson, Nanofluids: key parameters to enhance thermal conductivity and its applications, Appl. Therm. Eng. 207 (2022) 118202.
[73] Q.S. Mahdi, H.M. Jaffal, Experimental Investigation for the thermal performance of modified closed wet cooling tower, Al-Nahrain J. Eng. Sci. 19 (2016) 310–326.